

# Cumulative damage effects in different machining strategies for 2.5D laser micro structuring of polyimide

D. Ilie \*, C. Mullan, S. Favre, G. M. O'Connor, T. J. Glynn  
National Centre for Laser Applications, National University of Ireland, Galway

## ABSTRACT

Polymers play an important role in many applications such as microelectronics and medical devices. Micro-channels and shaped holes can be produced by 2.5D micro-structuring with excimer laser sources using mask projection. The industrial cost associated with these processes can be greatly reduced by the use of solid-state lasers due to their lower cost and maintenance. For this purpose, we investigate the interaction of polyimide (Kapton™) with solid-state lasers emitting in the UV (266 & 355 nm) spectral range. The study presents a comparison of the ablation profiles obtained for different laser sources and these are discussed in terms of roughness and efficiency. Limitations on the actual motion system (scan-head) are evident and the need to control the material removed by a small Gaussian beam in terms of overlapping for the direct writing process will be highlighted.

**Keywords:** polyimide, solid-state lasers, laser micro-processing

## 1. INTRODUCTION

Rapid expansion of industries based on micromachining led to an increased interest in laser based technologies in the last 10 years. Complex features are machined by 2.5D laser micromachining, which is typically a “subtractive” process with successive removal of thin layers to obtain the 3D feature. Until recently, 2.5D micromachining at an industrial scale was commonly performed on excimer lasers in lithography-based methods combined with chemical etching of the material exposed. In this technique the results were good in terms of features quality but the costs for maintenance and mask fabrication are high. Our work investigates diode pumped solid state (DPSS) lasers, at two different wavelengths, as potential sources for 2.5D micromachining by direct writing process. A comparison is made with excimer laser. Also, simple computer simulations based on ablation spot profiles obtained from a combination of ablation curve and beam profile are used for comparison with experimental results.

The objective of this study is to develop a high throughput laser ablative process for production of shaped features using DPSS technology.

## 2. EXPERIMENTAL PROCEDURES

### 2.1. Material

Due to its properties and wide range of use the material used is Kapton™ HN film, 125 µm thickness from Dupont®. This polyimide film possesses a stable combination of properties such as mechanical, physical, and electrical over a wide range of temperatures and has no melting point which makes it successfully used in various applications<sup>1</sup>. Polyimide is a strong absorber in the UV range with an absorption coefficient<sup>2</sup>  $a = 3.2 \times 10^5$  and has a good photo-machinability, low ablation threshold and small thermal loading<sup>3</sup>.

For experiments small rectangles of polyimide were cut and mounted on a silicon frame with an adhesive at the edges. This setup was used to avoid bending of the Kapton™ thin film.

### 2.2. Lasers

The excimer laser used for comparison with DPSS lasers is a commercial ATLEX–SPI operating at 193 nm wavelength, ArF medium, 3-7 ns pulse durations and a repetition rate up to 300 Hz. Pulse energy up to a maximum of 110 µJ can be set varying either repetition rate or the voltage discharged by the capacitors. Ablation is made through mask imaging of a

---

\* diana.ilie@nuigalway.ie; Phone +353 91 750469; Fax +353 91 750594; www.ncla.ie

flat top beam at a demagnification ratio between 1 and 10 controlled with two mirrors that change the optical path length. Afterwards, the beam passes through the focusing lens, reaching the work-piece. Two DPSS, Q-switched lasers emitting in the UV range have been used in this study, an AVIA 355-4500 from Coherent Inc. at 355 nm wavelength, repetition rate between 10 Hz and 100 kHz, maximum average output power of 4.5 W, and a HIPPO from Spectra Physics, at 266 nm wavelength, repetition rates from 30 kHz to 300 kHz, a maximum average output power of 2 W. For beam delivery and motion of the beam across the machining place both DPSS lasers are equipped with SCANLAB HurrySCAN<sup>®</sup> scan heads, systems made from two mirrors and F-Theta focusing lens, software controlled<sup>4</sup>.

In the case of DPSS lasers pulse energy can be set in different ways such as changing the repetition rate or the diode current. These changes could affect the beam profile, the pulse durations and the pulse to pulse stability<sup>5</sup>. To avoid this, a single set of parameters that gave the maximum pulse energy was used. For pulse energy adjustment at the workplace a combination of half - wave plate and polarized beam splitter was installed in the optical setup of the laser.

### 2.3. Measurements and analysis

The surface roughness was determined experimentally, using the root-mean-square (rms) error, which is an area-weighted statistic. Compared to arithmetical mean roughness (Ra) or peak valley (PV) the rms has the advantage of more accurately reflecting the optical performance of the surface being measured<sup>6</sup>.

The rms is calculated as the standard deviation of the height  $x_i$  (depth) of the test surfaces (or lines) relative to the reference  $x_0$  at all the data points  $n$ , in the interferogram.

$$rms = \sqrt{\frac{\sum_{i=1}^n (x_i - x_0)^2}{n}} \quad (1)$$

Visual observation and distance measurements were made using an Olympus optical microscope while depth, as far as possible, and rms measurements were done with ZYGO profilometer. To make all measurements possible with the profilometer all the samples had to be cleaned with ethanol after irradiation.

## 3. RESULTS AND DISCUSSION

To ensure a similar laser-matter interaction for all consecutive layers, each layer must have a precise and uniform depth with a good smoothness characterized here by rms values. As a reference, rms value for native Kapton<sup>TM</sup> given by the producer is 40 nm<sup>1</sup>, subject to variation as some values measured in our laboratory were as low as 25 nm.

The material removal from a single layer differs between excimer lasers and solid state lasers (imaging versus direct writing). We decided to characterize and compare layers having the same depth. These were obtained with each laser at the optimum predetermined parameters.

### 3.1. Solid state lasers

A layer removed with a solid-state laser is made by direct writing through a well defined control of the incident pulses. The overlap between small Gaussian beams in both the scanning direction and the perpendicular direction is set to be constant.

#### 3.1.1. Computer simulations

Computer simulations of “dry ablation” were carried out. The model results were compared with experimental results. The term “dry ablation” is used when the effects of melted material flow under plume pressure or inside the material at explosive boiling and decomposition of the polymer can be neglected<sup>7</sup>, which is the case with Kapton<sup>TM</sup><sup>1</sup>.

In the case of a symmetrical Gaussian beam, as is considered for DPSS lasers used in this study, the local irradiance was considered as follows:

$$I = I_0 * \exp\left(\frac{-2r^2}{w_0^2}\right) \quad (2)$$

where  $I_0$  is the irradiance at the centre and  $w_0$  is the radius at the point where the irradiance has dropped to  $I_0/e^2$ . Approximately almost 86% of the total power in the Gaussian beam in TEM<sub>00</sub> is considered in a spot diameter<sup>8</sup> of  $2w_0$ .

The machined Gaussian profile obtained experimentally by the interaction of a single laser pulse with the material at defined incident fluence was used as a model for computer simulation. Areas with overlaps between pulses ranging from

10% to 90% were generated in Matlab<sup>®</sup> and for each overlap; resulting roughness (rms) values and depth were extracted. By overlap here we mean the distance between centers of two consecutive craters given as a percent of their diameter. An example of a computer generated area, which is in fact a “negative” of the experimental machined result, is shown in Figure 1.

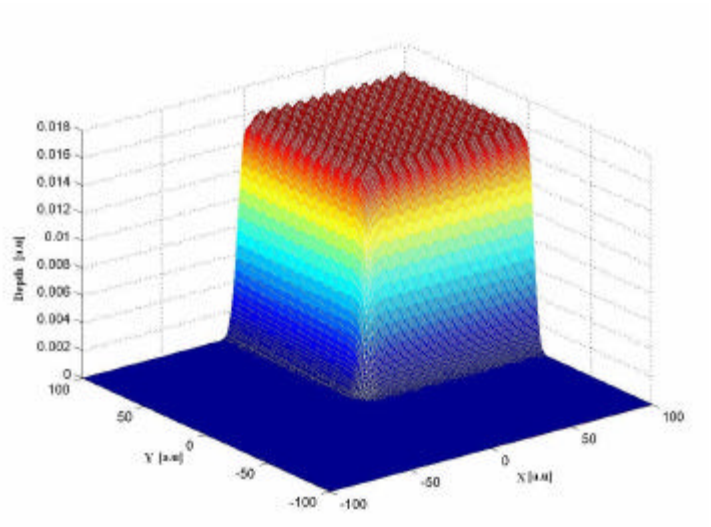


Figure 1: Area generated with overlapped Gaussian pulses in computer simulations

Figure 2 is constructed with results obtained from two sets of simulations based on the profiles of craters machined with single pulses at 266 nm wavelength laser in two different regimes, one at pulse energy of 5  $\mu\text{J}$  in focal plane that gave a measured depth of 1  $\mu\text{m}$  with a radius of 8  $\mu\text{m}$  (respectively used as  $I_0$  and  $w_0$  in equation 2) and the second one at 42  $\mu\text{J}$  pulse energy which gave a measured depth of 0.34  $\mu\text{m}$  with a radius of 50  $\mu\text{m}$ .

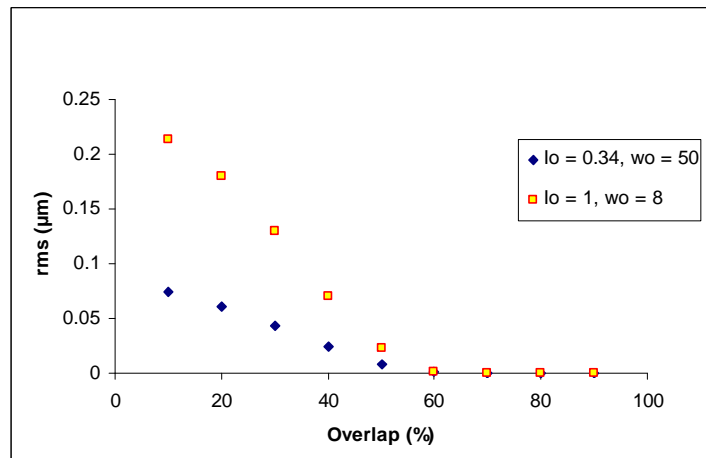


Figure 2: Rms evolution with overlap obtained in computer simulations based on measured profiles for craters machined with a single shot at two pulse energies: 5  $\mu\text{J}$  (a diameter of 16  $\mu\text{m}$  and a depth of 1  $\mu\text{m}$ ) and 42  $\mu\text{J}$  (diameter of 100  $\mu\text{m}$  and a depth of 0.13  $\mu\text{m}$ ).

In both cases the simulated roughness values decrease with overlap in the same manner, reaching a flat profile with quasi negligible rms values over 60% overlap. For a small overlap, it can also be observed that an increase in beam sharpness leads to an increase in roughness. This suggests that in the case of ablation, without taking in account the precise details of the laser-matter interaction, the surface profile in such simple simulations improves to reach a minimum for overlaps over 60%, leading to the presence of very smooth surfaces.

### 3.1.2. Experimental results

To characterize the lasers incident fluence, the spot size was measured with the Mylar method<sup>4</sup>. With lenses of focal length  $f = 100$  mm, the beam diameter at focal plane was determined to be respectively  $16.4 \mu\text{m}$  and  $29 \mu\text{m}$  for 266 nm and 355 nm laser, in both cases with a slightly elliptical shape ( $< 1.4$ ).

Areas with overlaps between machined craters in the range 10 % to 90% and laser fluence between  $0.12 \text{ J/cm}^2$  and  $22.38 \text{ J/cm}^2$  were machined in these conditions for direct comparison with our simulation. The post analysis and observation with the optical microscope and profilometer of the ablated surfaces obtained at focus showed a poor texture as presented in Figure 3, which deteriorated even more with an increase of the overlap ( $> 70\%$ ).

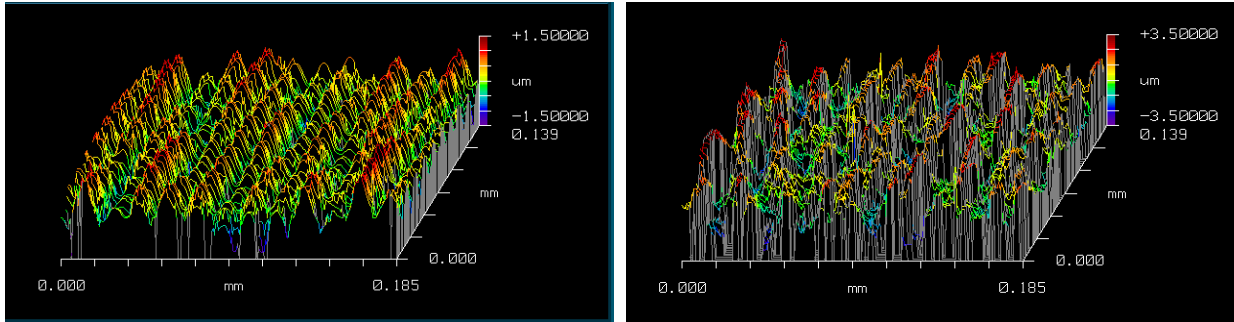


Figure 3: Profile of an area machined with 10 % overlap (left) and 60 % overlap (right) with a  $12 \text{ J/cm}^2$  laser fluence

The images of Figure 3 are the profiles of areas machined at focus with the 266 nm laser with a spot size of  $16.4 \mu\text{m}$  and a fluence of  $12 \text{ J/cm}^2$ . On the left hand side, the 10% overlap resulted in a depth of  $1.43 \mu\text{m}$  and a roughness of  $0.5 \mu\text{m}$  and on the right hand side, 60% overlap between pulses led to a depth of  $5.17 \mu\text{m}$  that resulted in a roughness of  $1.25 \mu\text{m}$ . As can be seen, the surface is not regular at all and further increase of the overlap gave worse results. Moreover, the surface presented in Figure 3b, with 60% overlap between pulses, accordingly to our simulation (Figure 2) should have a very smooth profile, better than the one obtained with 10 % overlap between pulses.

To try to understand the origin of this problem, we analyzed single line scanning onto Kapton<sup>TM</sup>. Data obtained for lines machined with two different machined spot sizes ( $w_o = 8 \mu\text{m}$  and  $w_o = 35 \mu\text{m}$ ) with parameters set to achieve the same depth per pulse,  $0.5 \mu\text{m}$ , are plotted in Figure 4. A similar behavior to the one predicted by the simulations (Figure 2) is observed for overlap values smaller than 60% in the case of small spot size and 70% overlap for the bigger spot diameter. However, a deviation from the perfect smoothness that should occur is obtained experimentally for large overlap.

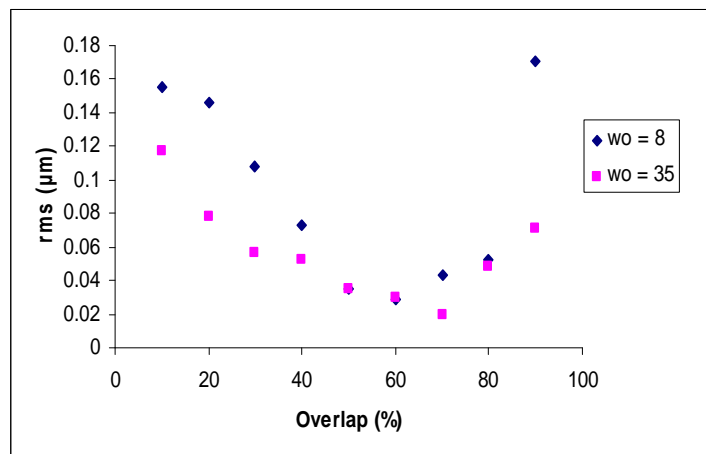


Figure 4: Overlap versus roughness for lines scanned with the 266 nm wavelength laser at two different spot sizes with the same depth of a single machined spot ( $0.5 \mu\text{m}$ ).

These early results led us to the supposition that for area machining with 60% overlap as presented in Figure 3, the motion system has some limitations. If we assume a smooth scanner movement the setting for overlap in scanning direction depends mostly on the repetition rate of pulse delivery<sup>9</sup>. This surface deterioration phenomenon could be attributed to the Galvanometer scan head resolution of  $\pm 2.5 \mu\text{m}$  compared to the small size of the focused spot that requires a motion on very small distances up to hundreds of nanometers to achieve a well defined overlap. To overcome this problem we decided to use a larger spot size. Experiments were carried out by machining  $2 \text{ mm}^2$  areas away from the focal plane where the incident measured machined spot size was in a range of  $70 \mu\text{m}$  to  $100 \mu\text{m}$  for the  $266 \text{ nm}$  laser and  $50 \mu\text{m}$  for the  $355 \text{ nm}$  laser. However, we should note that the usage of bigger spot size has some disadvantages like large wall angles and limited minimum feature size for the generation of 2.5D machining. With the new settings we were unable to determine the exact spot size with the Mylar method and only machined one was measured. For this reason, further results are not presented in terms of laser fluence and we will refer instead to pulse energy used. With such settings, we observed that smooth areas could be generated as is presented in Figure 5 with a closer detail of the ablated surface onto the left hand side, where resulting area's roughness value was  $94 \text{ nm}$  for 60% overlap with  $266 \text{ nm}$  laser.

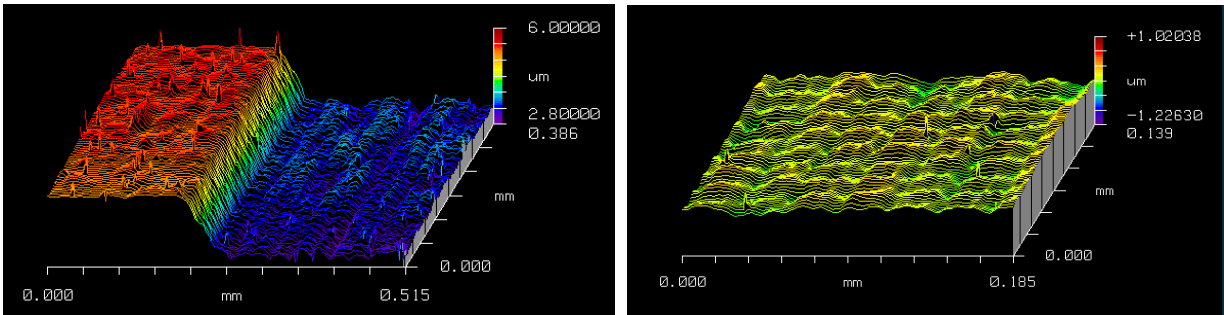


Figure 5: Edge (left) of a  $2 \mu\text{m}$  deep surface ablated with  $42 \mu\text{J}$  pulse energy at 60% overlap between pulses ( $70 \mu\text{m}$  spot diameter) resulting in a roughness of  $94 \text{ nm}$  as shown in its detail (right)

A plot of the surface rms results versus overlap in Figure 6 for both solid state lasers shows similar behavior with an improvement in rms until 60% overlap for  $266 \text{ nm}$  ( $50\%$  for  $355 \text{ nm}$ ), which is comparable with what computer simulations predicted (Figure 2). As rms also depends on depth, the two sets of data presented in the graph in Figure 6 are chosen for equal depths for crater machined with a single laser shot. The rms values obtained for areas with a specific overlap follow a similar trend to the one obtained for lines in Figure 4 but the values are slightly larger. The results suggest that the best texture is achieved for 60% overlap at  $266 \text{ nm}$  and 50% overlap at  $355 \text{ nm}$ .

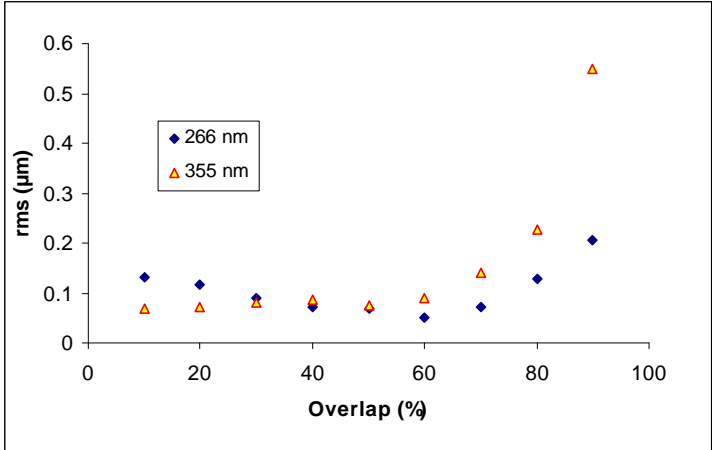


Figure 6: Experimental results of rms versus overlap for areas machined with respectively  $100 \mu\text{m}$  and  $50 \mu\text{m}$  spot size by DPSS lasers at two different wavelengths.

The remainder of this section will seek to identify reasons for why the rms roughness increases at high overlap. However, as observed for single line scanning, the situation is different when the overlap is further increased. While this should lead to an improvement of the surface texture, a deterioration is in fact observed. For specific experimental configurations, galvanometer effects can be excluded as the origin for such poor surface texture. For example in cases of high overlap with large laser spot diameters, the displacement of the galvanometer is large compared to its limiting accuracy and hence the jitter in mirror movement should not make a significant contribution to roughness. Re-deposition of laser-generated debris is also considered as making a possible contribution to roughness. Laser ablation of polyimide is primarily a photothermal process in the UV range. At these wavelengths previous studies showed that temperature at the laser-irradiated surface rises until it reaches vaporization and finally ablation occurs<sup>10</sup>. In this process of thermal decomposition, the carbon content increases while the oxygen and nitrogen content decrease. The formation of graphitic carbon and deposition of carbon with a more amorphous structure around the laser-ablated feature has been detected<sup>11,12,13,14,15</sup>. In multipulse exposure either in static or scanning beam irradiation, debris re-deposition from previous pulses and induced surface change render laser material interaction unpredictable<sup>15,16</sup>. Optical (Figure 7) and scanning electron microscopies revealed significant debris re-deposition on the ablated areas irradiated with over 70% overlap.

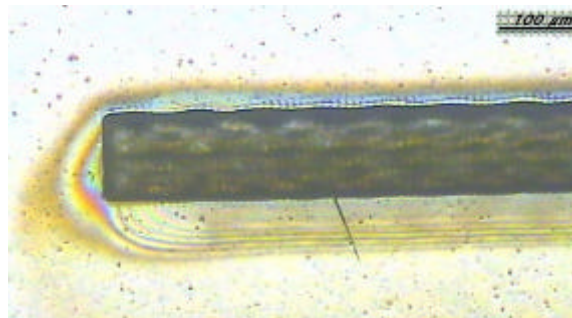


Figure 7: Image obtained with the optical microscope of an area machined with high overlap. Significant debris re-deposition outside and inside the area can be seen.

The quantity of debris resulting from the ablation process depends on the polyimide properties, working environment, laser fluence and wavelength<sup>9,16,17</sup>. For fixed laser fluence the comportment of the depth is highly dependent on overlap so the results obtained experimentally and by simulation have also been investigated and are presented in Figure 8.

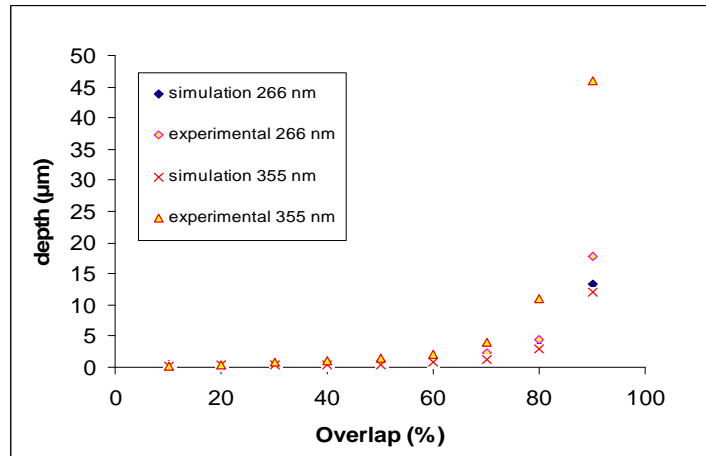


Figure 8: Comparison between depths obtained experimentally and in simulation for fixed pulse energy with diameters of 100 μm and 50 μm at respectively 266 nm and 355 nm.

It can be observed from Figure 8 that depth increases within the same behavior with overlap for both experimental results and computer simulations. Higher depths were obtained in experimental work and especially for high overlap (> 80%). A possible explanation could be given by the peripheral parts of the Gaussian beam. We suggest that they do not exceed ablation threshold for a single pulse but due to a cumulative effect, they make a contribution to material removal at high overlaps. In computer simulations (Figure 2) this effect is not taken in account.

Having established previously the overlaps for which the best surface texture can be experimentally obtained, the laser pulse energy required to obtain a desired depth with a smooth surface was determined. Plotting the depths obtained for a range of pulse energies with the two lasers suggests a linear behavior in this regime.

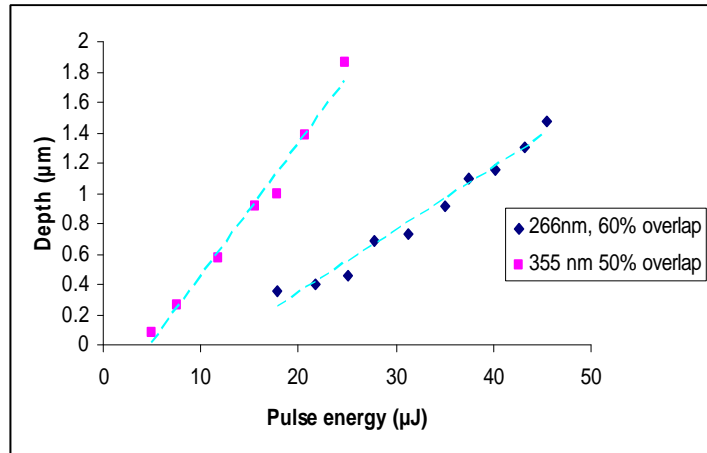


Figure 9: Depth variation with pulse energy for 266 and 355 nm wavelengths at 60% and 50% overlap for spot sizes of 100 µm and 50 µm respectively

Using the linear fits in Figure 9 we determined that pulse energy of respectively 55 µJ and 28 µJ is needed to produce a 2 µm deep layer at 266 nm and 355 nm.

The rms behavior also shows a quasi-linear relationship with the depth of the areas (Figure 10) and roughness values of respectively 94 nm and 131 nm at 266 nm and 355 nm could be achieved for a 2 µm deep layer.

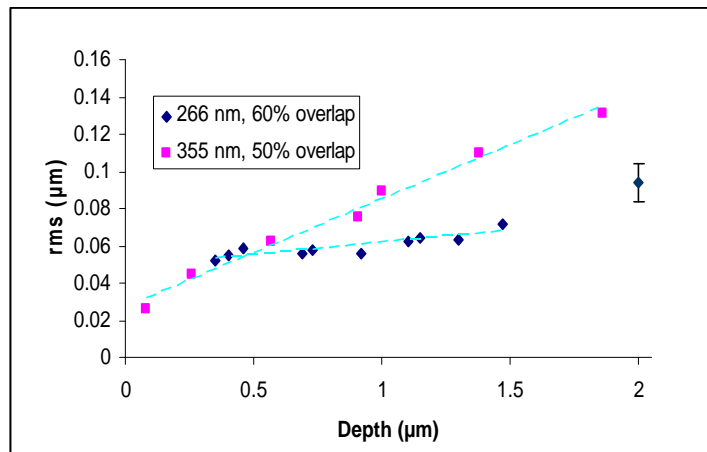


Figure 10: Rms evolution with depth of ablated layer at 60% overlap between pulses for the 266 nm laser and 50% overlap between pulses for the 355 nm laser.

In the frame of 2.5D machining, multiple pass layers have been investigated and step structures were achieved as presented in Figure 11.

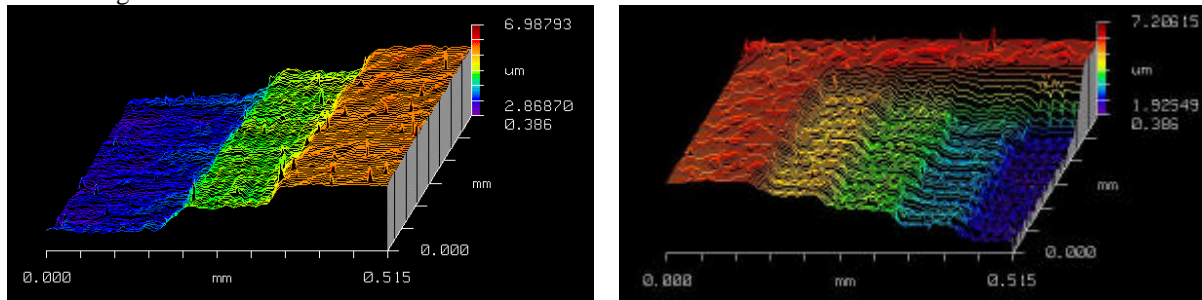


Figure 11: Example of two (left) and four (right) step layer achieved by 266 nm laser direct writing machining with a spot size of 70 μm.

As the depth increase and due to the multiple incident beams onto the surface by the number of passes, an increase of the roughness should be expected for subsequent machined features (Figure 10). To improve these results and as it should affect the resulting pattern as well, the dependence of the scanning direction has been investigated. The resulting values for alternative parallel and perpendicular scanning directions are reported in Figure 12.

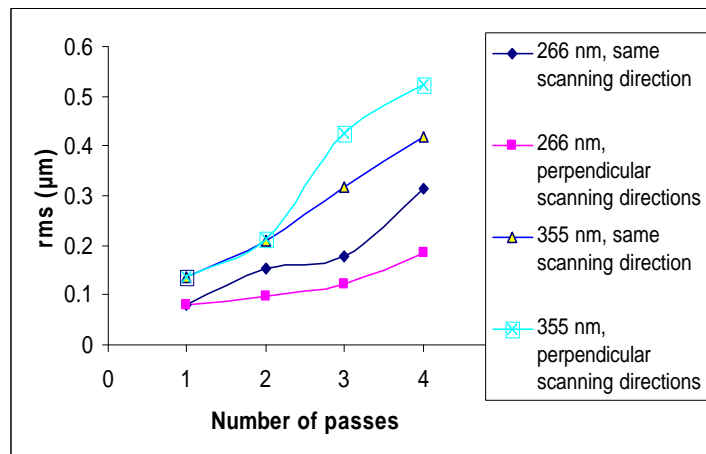


Figure 12: Rms evolution for multiple passes of different strategies with 100 μm and 50 μm spot of 266 nm and 355 nm laser with respectively 60% and 50% overlap.

It can be observed that when machining in multiple scans, irrespective of the machining strategy, rms increases with number of passes. Rms values for the fourth layer show different behavior for the two lasers. Further investigation needs to be done for analyzing the synchronization between the scanner and the laser to ensure that the machining method is similar for both lasers as it could be observed that for the 266 nm laser, a better machined area is achieved in perpendicular alternative scanning directions, which is the opposite of the 355 nm laser where resulting roughness is better by the use of the same direction.

### 3.2. Excimer laser

Material removal for a layer of a certain depth is made with multiple pulses imaging without relative motion between the sample and the laser beam.

This experiment was made for a range of laser fluence between 56 mJ/cm<sup>2</sup> and 332 mJ/cm<sup>2</sup> (maximum provided by the laser). For each laser fluence, circular holes of 200 μm diameter, with different number of pulses were machined to determine ablation rates and rms evolution with depth.

Results presented in Figure 13 show a linear dependency of ablation rate per pulse with laser fluence. Ablation rates per pulse are calculated by dividing the depth obtained by the number of pulses, 20 in this case.

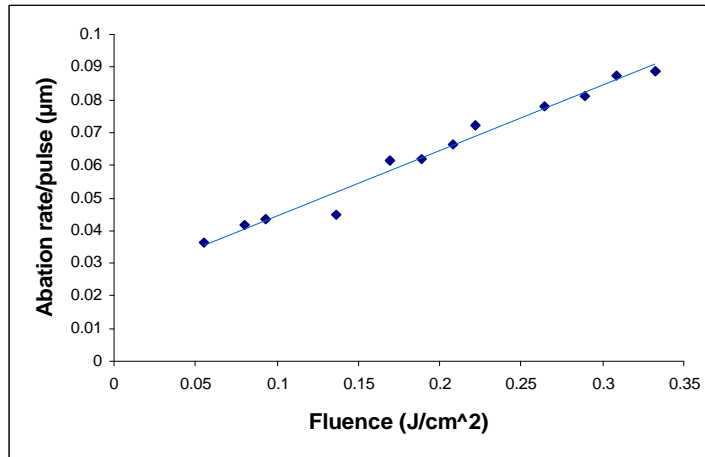


Figure 13: Ablation rate per pulse at different laser fluence.

A linear dependence appears as well, when rms values are plotted against depths obtained for each laser fluence but with different slopes, which decrease with fluence (Figure 14). For this reason, best results were obtained with the highest fluence used during the experiment ( $0.332 \text{ J/cm}^2$ ) and a roughness value of 113 nm is obtain at  $2 \mu\text{m}$  layer depth within these parameters.

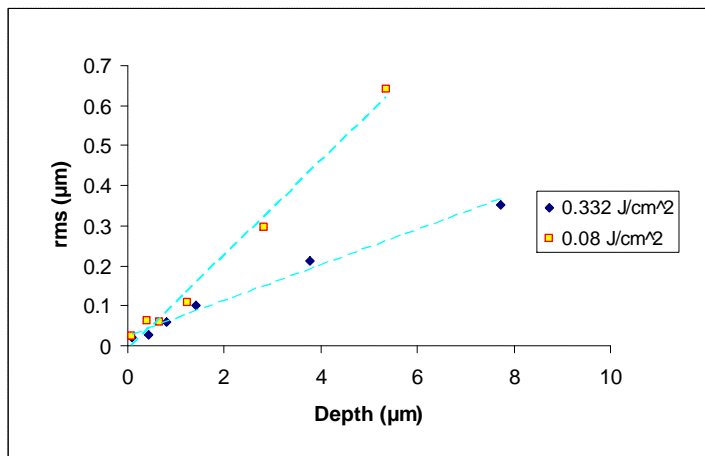


Figure 14: Rms variations with depth at two different laser fluence. The rms increases with depth in a linear mode.

An explanation for rms decrease with laser fluence is possible. SEM results revealed the presence of cone like structures. Some authors claim that these formations are generated by Ca impurities with a higher ablation threshold than Kapton™<sup>13</sup>. If the laser fluence is high enough the impurities are also ablated leaving a textured surface.

#### 4. SUMMARY AND CONCLUSIONS

In this paper we report results obtained in 2.5D micro-machining of polyimide (Kapton™) with different UV laser sources by direct comparison between results obtained for a  $2 \mu\text{m}$  deep layer.

Material removal of single layer for Excimer laser is made through mask imaging while for the DPSS lasers is made by scanning with a small Gaussian beam at a very well controlled distance between pulses. Excimer results show a surface texture linearly dependent on laser fluence used. A  $2 \mu\text{m}$  deep area with a surface rms of  $0.113 \mu\text{m}$  was obtained for the best experimental parameters.

The resulted texture of the ablated surface depends on different parameters such as wavelength, beam profile and incident energy for example. However, with the use of Gaussian shaped pulse intensity as emitted by solid-state lasers, the overlap between pulses, and resolution of the motion system should also be taken in account. For this purpose, we developed a simple model of “dry ablation” to predict the behavior of experiment.

We note a good match of experimental result with our model for low fluence and low overlap. However, a deviation of this sample model was observed for higher parameters. This deviation could be associated with several features such as motion system limitation, debris generation, and an incubation effect resulting from high density of low pulse energy onto the same area.

With the optimum parameters, different results for 355 nm and 266 nm have been observed. On a single scanned 2  $\mu\text{m}$  deep ablated area with 266 nm wavelength laser the minimum roughness value was 0.094  $\mu\text{m}$ . A 1.4 time higher rms value was obtained with the 355 nm laser as the roughness experimental value was 0.131  $\mu\text{m}$ . Further work will be performed in the future regarding these early results.

### ACKNOWLEDGEMENTS

The authors would like to acknowledge Enterprise Ireland for the financial support for this research through grant CFTD – 2003 330.

### REFERENCES

- 1 DUPONT, “Kapton-Summary of properties”.
- 2 N. Arnold, N. Bityurin, “ Model for laser-induced thermal degradation and ablation of polymers”, *Appl. Phys. A* **68**, 615-625 (1999).
- 3 W. S. Chang, B. S. Shin, J. Kim, K. H. Whang, “Photothermal three-dimensional fabrication of polymers using diode-pumped solid state lasers”, *JM3* **3**(3) 472-477 (July 2004).
- 4 H. Howard, A. Conneely, G. M. O’Connor, T. Glynn, “Investigation of a method for the determination of the focussed spot size of industrial laser beams based on the drilling of holes in Mylar film”, *Proceedings of SPIE* Vol. **4876**, 541-552 (2003).
- 5 K. Koechner, “*Solid-State Laser Engineering*”, 5th edition ed. (Springer-Verlag, Berlin Heidelberg, 1999).
- 6 Zygo corporation, “PV versus RMS”, Application Note
- 7 V.N. Tokarev, S. Lazare, C. Belin, D. Debarre, “Viscous flow and ablation pressure phenomena in nanosecond UV laser irradiation of polymers”, *Appl. Phys. A* **79**, 717-720 (2004).
- 8 James T. Luxon, David E. Parker, “*Industrial lasers and their applications*”, 2nd ed., Prentice - Hall International Editions, p125-128, 1992
- 9 K.C. Young, D.W. Zeng, T.M. Yue, “High repetition rate effect on the chemical characteristics and composition of Upilex-S polyimide ablated by a UVNd : YAG laser,” *Surface and Coatings Technology* **160** (1), 1-6 (2002).
- 10 John B. cooper, Benjamin Julian, Henry Morrison, Pang Song, Sacharia Albin, Jianli, Zheng, “Surface characterisation of pulsed UV-laser modified polyimide films”, *Thin Solid Films* **303**, 180-190 (1997)
- 11 T. Lippert, E. Ortelli, J. C. Panitz et al., "Imaging-XPS/Raman investigation on the carbonization of polyimide after irradiation at 308 nm," *Appl Phys a-Mater* **69**, S651-S654 (1999).
- 12 F. Raimondi, S. Abolhassani, R. Brutsch, F. Geiger, T. Lippert, J. Wambach, J. Wei, and A. Wokaun, “Quantification of polyimide carbonization after laser ablation” *J. App. Phys.*, **88**(6), 3659-3666 (2000).
- 13 K.C. Young, D.W. Zeng, T.M. Yue, “High repetition rate effect on the chemical characteristics and composition of Upilex-S polyimide ablated by a UVNd : YAG laser,” *Surface and Coatings Technology* **160** (1), 1-6 (2002).
- 14 Srinivasan, R. R. Hall, W. D. Loehle et al., "Chemical transformations of the polyimide Kapton brought about by ultraviolet laser radiation," *J Appl Phys* **78** (8), 4881-4887 (1995).
- 15 K.C. Young, D.W. Zeng, “Laser ablation of Upilex-S polyimide:influence of laser wavelength on chemical structure and composition in both ablated area and halo”, *Surface and Coatings Technology*, **145** 186-193 (2001).
- 16 M. Pervolaraky, P.E. Dyer, P. Monk, “Ablation studies using a diode-pumped Nd : YVO4 micro-laser”, *Appl. Phys. A* **79**, 849-854 (2004).
- 17 Arvi Kruuning, “Underwater and water assisted laser processing: Etching, cutting ad rarely used methods”, *Optics and Lasers in Engineering* **41**, 329-352 (2004)